Folded Substrate Integrated Waveguide Based Composite Right/Left-Handed Transmission Line and Its Application to Partial H-Plane Filters

Tao Yang, *Member, IEEE*, Pei-Ling Chi, *Member, IEEE*, Ruimin Xu, and Weigan Lin, *Senior Member, IEEE*

***Abstract*—Composite right/left-handed (CRLH) transmission line structures based on the folded substrate integrated waveguide (FSIW) are presented and discussed in this paper. This FSIW-based CRLH (FSIW-CRLH) transmission line exhibits much lower cut-off frequencies as compared to the ordinary FSIW of the same footprint, and furthermore, it requires only one-half width of the conventional substrate integrated waveguide (SIW) based CRLH (SIW-CRLH) transmission lines while possessing the same dispersion characteristics. In addition, the proposed structure offers the advantage of a high quality factor for preventing the guided-wave circuits from radiation as suffered in the previous open CRLH transmission line structures when operated in the fast-wave region. All of the aforementioned properties lend the proposed FSIW-based CRLH transmission lines best suited to miniaturized and guided-wave microwave applications. In this paper, a comprehensive study on the FSIW-CRLH transmission structures is conducted by means of its dispersion relation and Bloch impedance. In addition, two partial H-plane filters are implemented here to demonstrate the capabilities of miniaturization and high quality factor based on the proposed FSIW-CRLH structures. The resultant filters are shown to have about 80% size reduction as compared to the conventional FSIW filters, and 59% size reduction as compared to the SIW-CRLH filters. To the best of our knowledge, it is the first time that the partial H-plane filters are implemented utilizing both the dispersion behavior of the CRLH transmission structures and the structural benefits of the FSIW configuration.**

***Index Terms*—Composite right/left-handed (CRLH) transmission line, folded substrate integrated waveguide (FSIW), partial H-plane filters.**

I. Introduction

OVER the last decades, the left-handed (LH) metamaterials, or more specifically, the composite right/left-handed (CRLH) transmission line structures, have attracted considerable attention in microwave engineering communities due to their unique and advantageous features [1]–[4]. A big variety of CRLH transmission line structures were proposed to demonstrate the left-handed characteristics and applied for novel applications [5]–[12]. Fig. 1 illustrates the typical dispersion diagram of the CRLH transmission line that is under the balanced condition [13]. In this diagram, the region between frequencies f_1 and f_2 lies in the fast-wave region where radiation takes place and leaky-wave antennas that support continuous beam scanning from the backward to endfire direction can be realized [11]–[14]. However, when the guided-wave circuits are built with these open CRLH structures, such as the microstrip lines [5], [15]–[17] and the substrate integrated waveguide (SIW) structures [18], the fast-wave radiation phenomenon will add extra loss and introduce unwanted noise to the nearby system components, thus deteriorating overall performance. On the other hand, in the current closed types of CRLH transmission lines [7], [8], transmission energy is fully constrained in the waveguide so that radiation mechanism can be prohibited. This CRLH waveguide-type transmission lines are, however, very bulky for guided-wave applications.

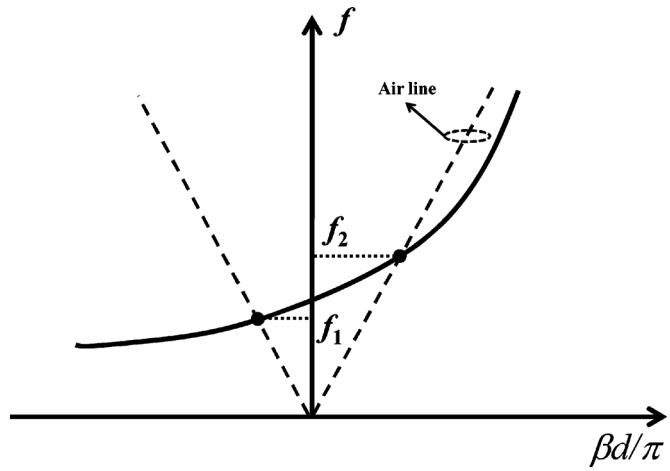

Fig. 1. Illustration of dispersion relation of the balanced CRLH transmission line (data from [13]).

The new type of waveguide structures, the folded substrate integrated waveguide (FSIW) [19], [20], provides a good solution to realize compact and artificial CRLH transmission lines that are best suited for the guided-wave applications with the need of a higher quality factor and better system electromagnetic compatibility (EMC). Fig. 2 shows the configuration of the FSIW along with its unfolded counterpart SIW. In addition to possessing high power handling capacity and integrability with the planar circuits as the SIW, the FSIW has only one-half width of

Manuscript received September 19, 2012; accepted November 08, 2012. Date of publication December 20, 2012; date of current version February 01, 2013. This work was supported by the National Natural Science Foundation of China under Grant 61201008, and by the National Science Council of Taiwan under Grant NSC 100-2218-E-009-027 and Grant NSC 101-2221-E-009-108.

T. Yang, R. Xu, and W. Lin are with the Department of Electrical Engineering, University of Electronic Science and Technology of China (UESTC), Chengdu 611731, China (e-mail: yangtao8314@gmail.com; rmxu@uestc.edu.cn).

P.-L. Chi is with the Department of Electrical and Computer Engineering, National Chiao Tung University, Hsinchu 300, Taiwan (e-mail: peilingchi@nctu.edu.tw).

Digital Object Identifier 10.1109/TMTT.2012.2231431

0018-9480/$31.00 © 2012 IEEE

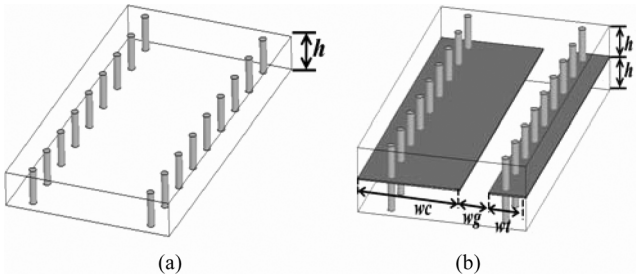

Fig. 2. Configurations of the SIW and FSIW. (a) SIW. (b) FSIW.

the unfolded size while maintaining the same dispersion characteristics [20]. Moreover, compared to SIW-based CRLH transmission structures, the closed configuration of the FSIW-CRLH transmission lines shows superiority in radiation loss suppression that is critical for guided-wave applications.

Similar to the FSIW structures, the partial H-plane filters were originally proposed in [21], [22] using the folded rectangular waveguides with only one-half width of the conventional H-plane filters. The partial H-plane filters implemented using the FSIW structures [23], [24] are able to show further height reduction. However, in both cases, less improvement is made in length reduction. In [13], a FSIW-based CRLH structure was proposed for antenna applications and flexible polarization ability was demonstrated using the same structure. However, the high quality factor of the FSIW-based CRLH structure, which is best applied for guided-wave implementation, limits the radiation efficiency of the leaky-wave antenna and results in low antenna gains in [13]. In addition, the full characterization and general design concept of the FSIW-based CRLH transmission line was not investigated and developed in [13].

In this paper, the FSIW structure is adapted to CRLH guided-wave applications. A comprehensive characterization for the FSIW-based CRLH transmission line is performed and a generalized parameter-extraction process is proposed to complete the design procedure. It can be shown that the FSIW-CRLH structure is able to extend its passband much lower than the cutoff frequency of the ordinary FSIW structure, showing the potential for miniaturization. Meanwhile, the proposed FSIW-CRLH is a closed structure that avoids radiation loss and suppresses noise coupling in the systems. To demonstrate the advantages in terms of compactness and high quality factor, the proposed FSIW-CRLH unit cell is used for the partial H-plane filter resonators that resonate at negative order modes, and two types of partial H-plane filters were constructed. Both the theoretic analysis and experimental results are given. The resultant H-plane filters exhibit significant length reductions and the overall footprint size is about 80% reduced as compared to the conventional FSIW partial H-plane filters. To the best of our knowledge, it is the first time that the partial H-plane filters are implemented utilizing both the dispersion behavior of the CRLH transmission structures and the structural benefits of the FSIW configuration.

II. Closed CRLH Transmission-Line Structure Based on the FSIW

Fig. 3 illustrates the proposed CRLH transmission line unit cell based on the FSIW. The interdigital fingers are etched in the middle metal plane of the FSIW. The middle metal plane is

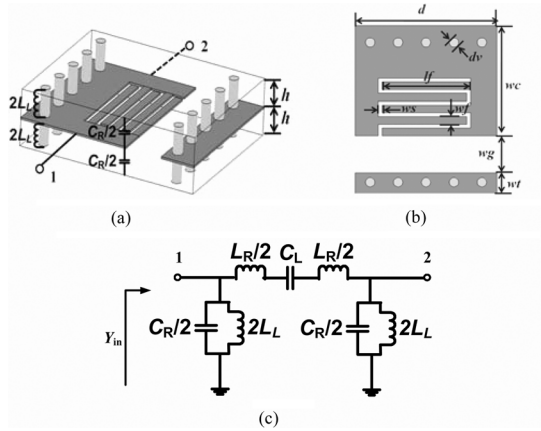

Fig. 3. (a) 3-D view of the unit cell for the proposed CRLH transmission line based on the FSIW. (b) Top view of the middle metal layer in the unit cell. (c) Equivalent circuit model for the unit cell.

connected through the metallic vias to the top and bottom metal planes, which are not shown here for better clarity of the interior details. Fig. 3(a) and (b) shows the 3-D view of the unit cell for the CRLH transmission line based on the FSIW and the top view of the middle metal plane in the unit cell, respectively. This proposed structure can be modeled using a symmetric CRLH equivalent circuit given in Fig. 3(c). The slots between the interdigital fingers in the middle metal plane give rise to the left-handed capacitance $(C_{\rm L})$ while the distributed inductance of the interdigital fingers contributes to the right-handed inductance $(L_{\rm R})$. The left-handed inductance $(L_{\rm L})$ comes from the metallic vias that connect the three metal planes in the FSIW, and the right-handed capacitance $(C_{\rm R})$ results from the capacitance between the middle metal layer and the top/bottom metal planes of the FSIW. In this equivalent circuit, the left-handed capacitance can be easily changed by varying the width and length of the slots while the flexible shunt inductance $L_{\rm L}$ can be obtained by choosing different waveguide widths and the substrate thickness.

Based on the equivalent circuit model in Fig. 3(c), the dispersion relation can be obtained by using the following (4):

$$\beta = \frac{1}{d}\cos^{-1}\left[1 - \frac{\omega^2}{2\omega_R^2} - \frac{\omega_L^2}{2\omega^2} + \left(\frac{1}{\omega_{\rm sh}^2} + \frac{1}{\omega_{\rm se}^2}\right)\frac{\omega_L^2}{2}\right] \quad (1)$$

where β is the propagation constant, d is the length of the unit cell, the $\omega_{\rm sh}$ and $\omega_{\rm se}$ represent the shunt and series resonant frequencies, respectively, and are given as follows:

$$\omega_{\rm sh} = \frac{1}{\sqrt{C_R L_L}} = 2\pi f_{\rm sh} \quad \omega_{\rm se} = \frac{1}{\sqrt{C_L L_R}} = 2\pi f_{\rm se}. \quad (2)$$

ω_R and $\omega_{\rm L}$are given as follows:

$$\omega_R = \frac{1}{\sqrt{C_R L_R}} = 2\pi f_R \quad \omega_L = \frac{1}{\sqrt{C_L L_L}} = 2\pi f_L. \quad (3)$$

To obtain the dispersion relation of the proposed structure, the periodic boundary condition is applied to the proposed unit cell, and the unit cell is simulated in the EM simulator, the Ansoft HFSS 12. The structural parameters of the unit cell are shown in

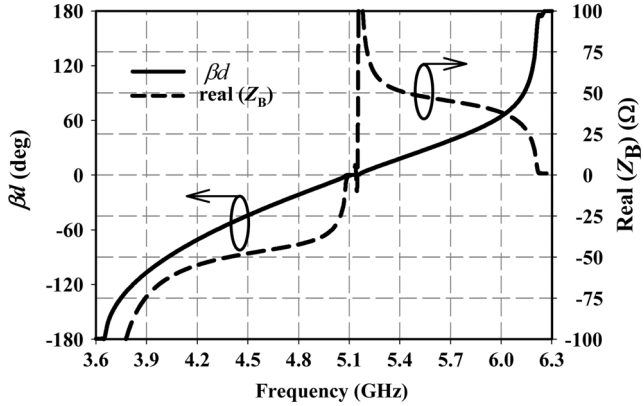

Fig. 4. Dispersion relation and Bloch impedance of the proposed unit cell.

TABLE I
PHYSICAL DIMENSIONS OF THE SIMULATED UNIT CELL. UNIT: MILLIMETERS

d	*lf*	*wc*	*wf*	*wg*	*ws*	*dv*	*wt*	*h*
8.72	5.9	6.6	0.5	2.9	0.22	0.6	1.2	0.508

Table I. Here, two layers of the Rogers 5880 substrates with the dielectric constant of 2.2 and thickness of 0.508 mm are used for simulation, and a thin film with a dielectric constant of 4.4 and a thickness of 0.07 mm is used between the two substrates for modeling the bonding film to assemble the two substrates. The calculated dispersion diagram is shown in Fig. 4. From the dispersion curve, the left-handed property is observed from 3.6 to 5.15 GHz where the phase velocity is anti-parallel to the group velocity. From 5.15 to 6.2 GHz, the right-handed phenomenon takes place where the phase velocity is parallel to the group velocity. In addition, the Bloch impedance that is used to characterize the impedance of the proposed unit cell in a periodic transmission structure was calculated by using the method given in [25]. Fig. 4 includes the real part of the Bloch impedance for the proposed unit cell. Negative Bloch impedance appears from 3.6 to 5.15 GHz, indicating a negatively traveling waves (or backward traveling wave), while the positive Bloch impedance from 5.15 to 6.2 GHz represents a positively traveling wave (or forward traveling wave). It is found that the magnitude of the Bloch impedance in the left-handed or right-handed region is close to 50 Ω, which ensures good impedance matching for the entire passband.

Based on the proposed unit cell, a FSIW-CRLH transmission line can be constructed by cascading several such cells. Fig. 5 shows the FSIW-CRLH transmission line with five aforementioned unit cells. To feed the transmission line, striplines are used at the two ends. The simulated reflection and transmission coefficients of this transmission line are shown in Fig. 6. As observed, in the passband that covers both the left-handed and right-handed regions, the reflection coefficient is below −10 dB, enabling the closed transmission line structure to be well applied to the guided-wave applications. For comparison purpose, a conventional FSIW as shown in Fig. 2(b) was simulated using the same waveguide parameters as those of the proposed FSIW-based CRLH transmission line. Fig. 7 shows the calculated *S*-parameters of the conventional FSIW. It is clear that the cutoff frequency of the proposed FSIW-CRLH

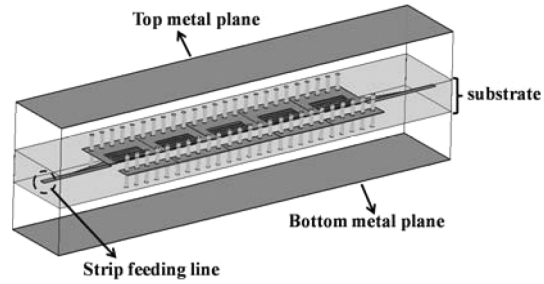

Fig. 5. Structure of the proposed CRLH transmission line based on the FSIW.

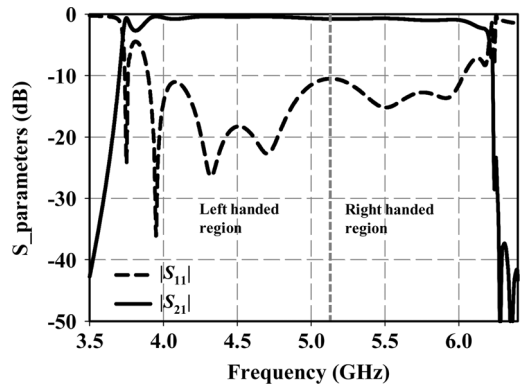

Fig. 6. Simulated *S*-parameters for the proposed CRLH transmission line based on the FSIW structure.

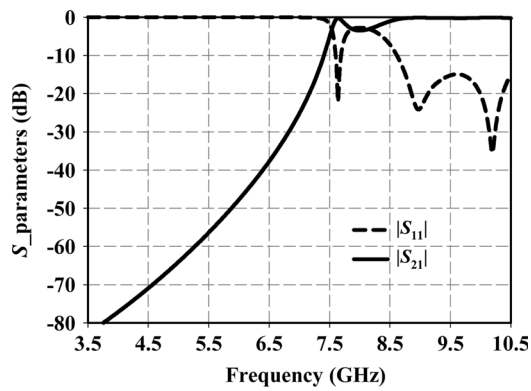

Fig. 7. Simulated *S*-parameters for the conventional FSIW with the same size of the proposed FSIW-CRLH transmission line.

transmission structure is much reduced from around 7.5 to 3.6 GHz that corresponds to the lower passband edge of the CRLH transmission line. The downward shift of the operating passband indicates the potential of the proposed structure for size reduction.

It should be noted that the proposed FSIW-based CRLH transmission line here is a closed structure. It is able to suppress the radiation loss in the fast-wave region that exists in an open CRLH transmission line such as [5] and [18], and is therefore best suited for implementing microwave systems that require high quality factor and high electromagnetic compatibility (EMC).

III. RESONATOR DESIGN BASED ON THE FSIW-CRLH UNIT CELL

The unit cell of the proposed FSIW-CRLH transmission line in Fig. 3 can be used to build the resonator in filter designs. Considering the equivalent circuit which is open-ended at its

TABLE II
PHYSICAL DIMENSIONS OF THE RESONATOR AND EXTRACTED VALUES OF THE LUMPED ELEMENTS

	d	lf	wc	wf	dv	wg	ws	wt	h	C_R	C_L	L_R	L_L	f_2	f_3	f_{sh}	f_{se}
Resonator	5.4 mm	3 mm	5.7 mm	0.5 mm	0.8 mm	1 mm	0.2 mm	1.2 mm	0.508 mm	1.676 pF	0.1776 pF	2.368 nH	0.2998 nH	5.3 GHz	10.39 GHz	7.1 GHz	7.76 GHz

Note: $f_2=\omega_2/2\pi$, $f_3=\omega_3/2\pi$, $f_{sh}=\omega_{sh}/2\pi$, and $f_{se}=\omega_{se}/2\pi$.

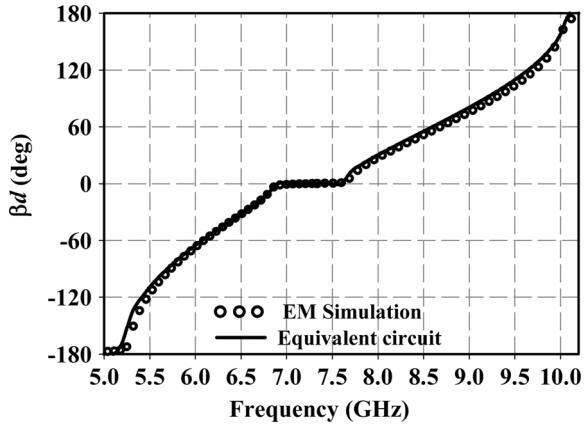

Fig. 8. Extracted dispersion diagram based on the EM simulation and the respective equivalent circuit.

two sides in Fig. 3(c), the input admittance ($Y_{\rm in}$) looking into one side can be expressed as follows:

$$Y_{\rm in}=j\frac{\left(\omega^2-\omega_{\rm sh}^2\right)\left[\omega^4-\left(\omega_{se}^2+\omega_{\rm sh}^2+4\frac{\omega_{\rm sh}^2\omega_{\rm se}^2}{\omega_L^2}\right)\omega^2+\omega_{\rm se}^2\omega_{\rm sh}^2\right]}{2\omega\omega_{\rm sh}^2L_L\left[\omega^4-\left(\omega_{\rm se}^2+\omega_{\rm sh}^2+2\frac{\omega_{\rm sh}^2\omega_{\rm se}^2}{\omega_L^2}\right)\omega^2+\omega_{\rm se}^2\omega_{\rm sh}^2\right]}. \tag{4}$$

The resonant frequencies of this unit cell can be obtained by solving the equation of the $Y_{\rm in}=0$, and can be calculated as follows:

$$\omega_1^2=\omega_{\rm sh}^2 \tag{5}$$

$$\omega_{2,3}^2=\frac{\omega_{\rm se}^2+\omega_{\rm sh}^2+4\frac{\omega_{\rm sh}^2\omega_{\rm se}^2}{\omega_L^2}\pm\sqrt{\left(\omega_{\rm se}^2+\omega_{\rm sh}^2+4\frac{\omega_{\rm sh}^2\omega_{\rm se}^2}{\omega_L^2}\right)^2-4\omega_{\rm se}^2\omega_{\rm sh}^2}}{2} \tag{6}$$

where ω_1,ω_2 and ω_3 are the three positive roots for $Y_{\rm in}=0$ and represent the three fundamental resonant frequencies of the open-ended unit cell. From (2) and (5), it can be found that one of the resonant frequencies, ω_1, occurs at the shunt resonant frequency of the unit cell and corresponds to the frequency where $\beta d=0$ in the dispersion diagram. On the other hand, let us assign $\beta d=\pm\pi$ and substitute it into the dispersion equation in (1), the following equation can be obtained:

$$\omega^4-\left(\omega_{\rm se}^2+\omega_{\rm sh}^2+4\frac{\omega_{\rm sh}^2\omega_{\rm se}^2}{\omega_L^2}\right)\omega^2+\omega_{\rm se}^2\omega_{\rm sh}^2=0. \tag{7}$$

It is found that the roots of (7) are exactly the same as (6). This implies that the other two resonant frequencies of the proposed resonator, ω_2 and ω_3, occur at the cut-off frequencies of the unit cell [4], and correspond to the frequencies where $\beta{\rm d}=-\pi$ and $\beta{\rm d}=\pi$ in the dispersion diagram, respectively. Both the resonances at ω_2 and ω_3 will behave as a half-wave resonator, but with different electrical wavelengths of $-\pi$ and π, respectively. Generally, the resonance at ω_1 with $\beta d=0$ is termed as zeroth order resonance, while the resonances at ω_2 with $\beta d=-\pi$ and ω_3 with $\beta d=\pi$ are termed as $-1^{\rm st}$ order resonance and $+1^{\rm st}$ order resonance, respectively.

For better investigating the resonant properties of the proposed resonator, a parameter-extraction process is used here to obtain the lumped-element values of the equivalent circuit. Firstly, a periodic boundary condition is applied at both terminals of the proposed unit cell in Fig. 3(a) to get the dispersion relation from the EM simulation. Then, the $-1^{\rm st}$ order resonant frequency ω_2 can be read from the dispersion diagram at the frequency where $\beta{\rm d}=-\pi$. The shunt resonant frequency $\omega_{\rm sh}$ and the series resonant frequency $\omega_{\rm se}$ can be directly read from the dispersion diagram at the two edges of the stopband where $\beta{\rm d}=0$, and it will be shown later how to distinguish these two band-edge frequencies. Theoretically, the $+1^{\rm st}$ order resonant frequency ω_3 can be also read from the dispersion diagram at the frequency where $\beta d=\pi$. However, the $+1^{\rm st}$ order resonance may be sometimes higher than the higher spurious resonance modes, such as the self-resonance of the interdigital fingers, thus, it may be difficult to be identified from the dispersion diagram. Instead, the ω_3 can be calculated by

$$\omega_3^2=\frac{\omega_{\rm sh}^2\omega_{\rm se}^2}{\omega_2^2}. \tag{8}$$

After the $\omega_{\rm sh},\omega_{\rm se},\omega_2$ and ω_3 are obtained, the $\omega_{\rm L}$ can be then calculated as

$$\omega_L^2=\frac{4\omega_{\rm sh}^2\omega_{\rm se}^2}{\omega_2^2+\omega_3^2-\omega_{\rm se}^2-\omega_{\rm sh}^2}. \tag{9}$$

Then, the left-handed inductance $L_{\rm L}$ can be obtained from (10)

$$L_L=j\frac{\left(\omega^2-\omega_{\rm sh}^2\right)\left[\omega^4-\left(\omega_{\rm se}^2+\omega_{\rm sh}^2+4\frac{\omega_{\rm sh}^2\omega_{\rm se}^2}{\omega_L^2}\right)\omega^2+\omega_{\rm se}^2\omega_{\rm sh}^2\right]}{2\omega\omega_{\rm sh}^2Y_{\rm in}\left[\omega^4-\left(\omega_{\rm se}^2+\omega_{\rm sh}^2+2\frac{\omega_{\rm sh}^2\omega_{\rm se}^2}{\omega_L^2}\right)\omega^2+\omega_{\rm se}^2\omega_{\rm sh}^2\right]} \tag{10}$$

where $Y_{\rm in}$ is the input admittance at an arbitrary frequency ω. To obtain $Y_{\rm in}$, a short section of microstrip line is tapped to one open side of the proposed resonator as an input port and simulated in the EM simulator (Ansoft HFSS). By de-embedding the phase reference plane and subtracting the phase shift introduced by the feeding microstrip line, the input admittance $Y_{\rm in}$ are calculated. By checking the input admittance at $\omega_{\rm se}$ and $\omega_{\rm sh}$, the $\omega_{\rm sh}$ can be identified with $Y_{\rm in}=0$. After $\omega_{\rm sh}$ is identified, $L_{\rm L}$

can be obtained from (10). Consequently, the values of the rest lumped elements in the equivalent circuit can be calculated as

$$C_R = \frac{1}{L_L \omega_{\rm sh}^2} \quad C_L = \frac{1}{L_L \omega_L^2} \quad L_R = \frac{1}{C_L \omega_{\rm se}^2}. \tag{11}$$

To give an example, Table II gives the dimensions of the proposed resonator and the extracted values for the lumped elements in the equivalent circuit. Fig. 8 shows the calculated dispersion curves based on the EM simulation and the extracted lumped-element values in the equivalent circuit. Excellent agreement is observed. This result validates the feasibility of the analysis approach and the equivalent circuit model of the proposed resonators. The -1st order resonance occurs at 5.3 GHz, while the zeroth order resonance and $+1$st order resonance take place at 7.1 and 10.39 GHz, respectively.

Since the -1st order resonance with an electrical length of $-\pi$ has much lower resonant frequency than the conventional half-wave resonance with an electrical length of π, it will have much smaller size and large potential of miniaturization capability in microwave applications. In the following sections, the -1st order resonance of the proposed CRLH unit cell in the FSIW structure will be used for resonators in miniaturized partial H-plane filters to demonstrate the guided-wave application of the proposed FSIW-CRLH structure. Two types of partial H-plane filters are proposed in the following section.

IV. Partial H-Plane Filter Designs

A. Fourth-Order Bandpass Filter With H-Plane Slots

Fig. 9 gives the first type of bandpass filters based on the proposed FSIW-CRLH transmission line structure. It consists of four CRLH unit cells shown in Fig. 3 and are indicated as Res. 1, Res. 2, Res. 3, and Res. 4 in Fig. 9(b). Each unit cell acts as a resonator and is designed to resonate at the $-1^{\rm st}$ order mode. The resonant frequency can be roughly decided from its dispersion diagram at the frequency where $\beta {\rm d} = -\pi$. An H-plane slot is introduced between two adjacent resonators for interstage coupling. These H-plane slots will behave as reactive coupling components, and have a π-type equivalent circuit shown in Fig. 10(a) [26]. The amount of coupling between two adjacent resonators or the reactance values in the equivalent circuit of Fig. 10(a) can be adjusted by controlling the width (w_1 and w_2) and length (s_1 and s_2) of the H-plane slots. Two tapped microstrip lines are placed beside Res. 1 and Res. 4 as the input/output ports, respectively. The amount of coupling between the input/output and the tapped resonators can be adjusted by changing the position of the tapped input/output lines. For the implementation convenience for the microstrip feeding lines, the top substrate is made to be shorter than the bottom substrate. The schematic diagram of the proposed filter is shown in Fig. 10(b), where the Q_e is the external quality factor of the Res. 1 and Res. 4 for input/output coupling, and theM_{12}, M_{23}, and M_{34} are the interstage coupling between adjacent resonators. For a symmetric structure, M_{12} is equal to M_{34}.

The center frequency of the filter is designed at 5.3 GHz. A Chebyshev low-pass prototype with a ripple level of 0.04 dB and a fractional bandwidth of 6% is used for the filter design, and the design process follows the direct-coupling method from [27].

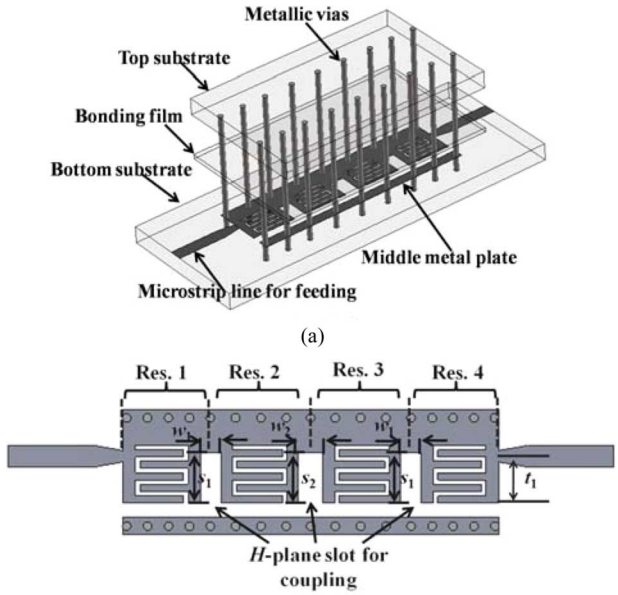

Fig. 9. Structure of the first type of the partial H-plane filters based on the proposed FSIW-CRLH structure. (a) 3-D view. (b) Top view of the middle metal layer.

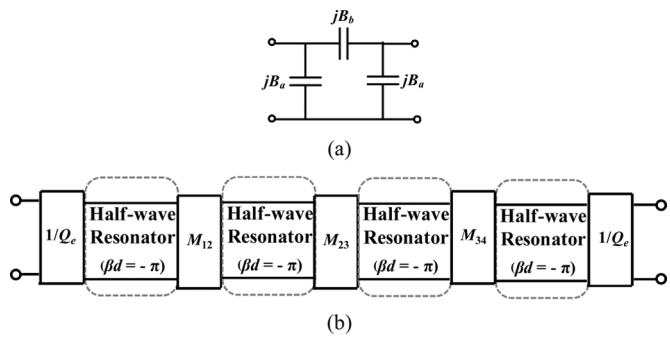

Fig. 10. (a) Equivalent circuit for the H-plane slot. (b) Schematic diagram for the partial H-plane filter.

Firstly, the length of the interdigital finger in each resonator is adjusted to get the resonant frequency at 5.3 GHz. The dimensions of the resonators is the same as those shown in Table II, and the dispersion relation extracted from the commercial EM simulator for the resonators is shown in Fig. 8. In the dispersion diagram, the resonance at 5.3 GHz approximately corresponds to the lower cutoff frequency where $\beta {\rm d} = -\pi$. The second and third fundamental resonances occur at 7.1 and 10.4 GHz, respectively. These two resonances will appear as the spurious passbands for the designed filter.

After the resonant frequency of each resonator is fixed, the interstage coupling coefficients and external quality factor are then extracted [27]. Thus, an initial filter is synthesized, and the optimization is then applied to the initial filter to get final performance. The required interstage coupling matrix M and external quality factor $Q_{\rm e}$ according to the low-pass prototype is given in (12)

$$M = \begin{bmatrix} 0 & 0.055 & 0 & 0 \\ 0.055 & 0 & 0.042 & 0 \\ 0 & 0.042 & 0 & 0.055 \\ 0 & 0 & 0.055 & 0 \end{bmatrix} \quad Q_e = 15.29. \tag{12}$$

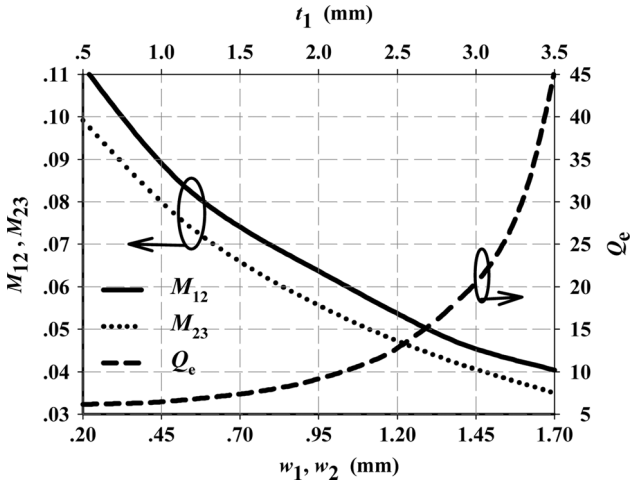

Fig. 11. Extracted interstage coupling coefficients between adjacent resonators and the external quality factor for the input/output coupling.

Fig. 11 gives the extracted interstage coupling coefficients between adjacent resonators and the external quality factor for the input/output coupling with respect to the corresponding physical dimensions. The physical dimensions for the required coupling coefficients and Q_{e} in (12) can be directly read from this figure.

The filter was fabricated on the Rogers 5880 substrate with the dielectric constant of 2.2 and loss tangent of 0.0009. Since two layers of such substrate with a thickness of 0.508 mm are stacked for the proposed FSIW-CRLH structure, a middle dielectric layer with the thickness of 0.07 mm, the dielectric constant of 4.4 and the dielectric loss tangent of 0.02 is used to model the bonding film between the two substrates, as shown in Fig. 9(a). The fabricated filter was measured with a network analyzer and a short-open-load-through (SOLT) calibration method is applied to eliminate the uncertainty errors from the network analyzer. Fig. 12 shows the simulation and measurement results for the first filter. As observed, good filter performance is obtained and the measured results agree well with the simulated results. The center frequency is around 5.3 GHz and the 3-dB fractional bandwidth is about 6.2%. The reflection coefficient is less than -15 dB in the passband. The passband insertion loss for the simulation is around 3.5 dB, whereas the insertion loss for the measurement is around 4.3 dB. The discrepancy between simulation and measurement may be ascribed to the deviation of the dielectric loss tangent of the substrate and bonding film. In addition, the losses from the SMA connectors and soldering, which are not included in the simulation, will also contribute to this discrepancy.

The high insertion losses obtained in both the simulation and the measurement are mainly due to the loss from the bonding film that has a high dielectric loss tangent on the order of 0.02. Due to the limited fabrication facility, the only available bonding film has high dielectric loss tangent. However, the proposed filter prototype with decent performance can be obtained when resorting to the Rogers 3001 bonding film with a much smaller loss tangent of 0.003 as reported in [28]. Fig. 13 shows the simulated $|S_{21}|$ of the filter in the passband using bonding films with the dielectric loss tangents of 0.02 and 0.003. As observed, the insertion loss in the passband can be reduced by

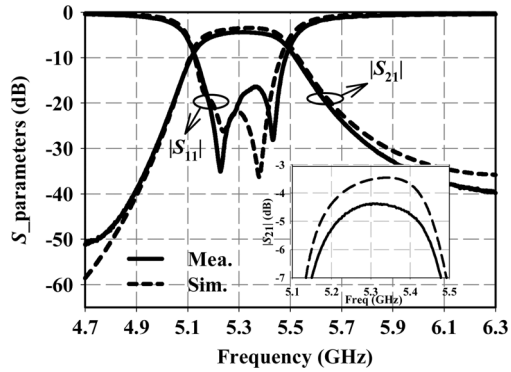

Fig. 12. Simulated and measured results of the bandpass filter with H-plane slots.

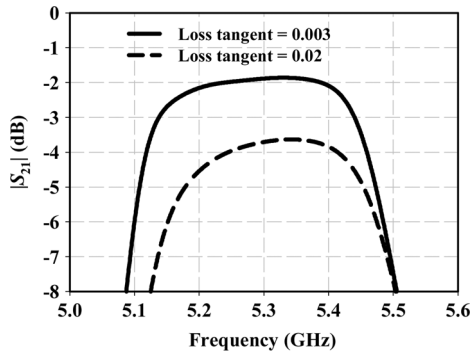

Fig. 13. Simulated $|S_{21}|$ in the passband by using the bonding films with the dielectric loss tangents of 0.02 and 0.003.

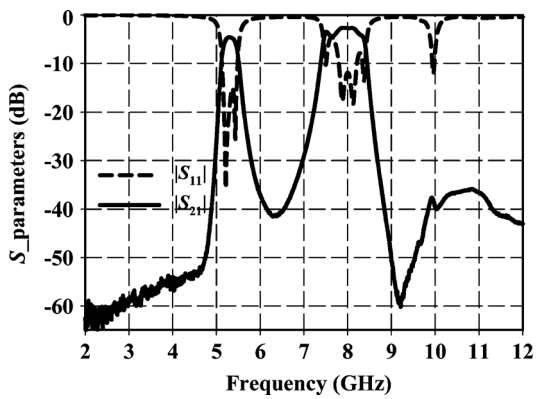

Fig. 14. Measured wide-band responses of the first type of the partial H-plane filters.

about 2 dB if the bonding film with the dielectric loss tangent of 0.003 is used. The unloaded quality factor (Q_{u}) of the proposed resonator can be extracted based on the insertion loss in the passband of the filter [27]. The extracted results show that the Q_{u} will increase from 73 to 176 if the dielectric loss tangent of the bonding film decreases from 0.02 to 0.003.

The measured wide-band performance of the proposed filter is shown in Fig. 14. As expected, the second spurious passband occurs around 7.1 GHz, resulting from the zeroth order resonance of the resonator and the third spurious passband resulted from the $+1$st order resonance occurs at around 10.4 GHz. The size of the filter is about 26 $\times$ 7.9 mm $(0.68\lambda_{\mathrm{g}} \times 0.21\lambda_{\mathrm{g}})$, not including the input and output feeding lines.

To give an idea on the capability of the proposed filter for achieving size reduction and a high quality factor, Table III

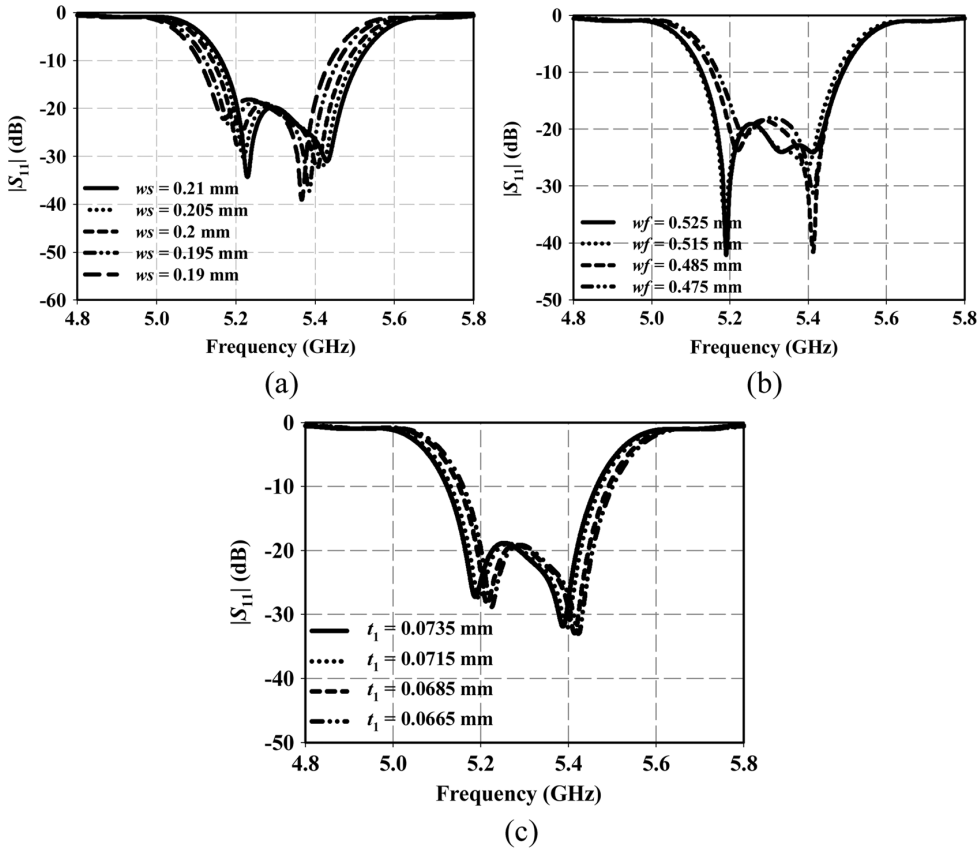

Fig. 15. Simulated filter sensitivity to the physical dimensions. (a) Simulated $|S_{11}|$ versus the variation of ws, (b) simulated $|S_{11}|$ versus the variation of wf; and (c) simulated $|S_{11}|$ versus the variation of t_1. Note that the values for these three parameters in fabrication were chosen as $ws = 0.2$ mm, $wf = 0.5$ mm, and $t_1 = 0.07$ mm.

TABLE III
COMPARISON WITH OTHER WORKS

		Filter order	*Band width*	*Insertion loss*	Q_u	*Size*
SIW-CRLH Filter 1 in [18]		2	6.5%	1.59 dB	50	Not available
SIW-CRLH Filter 2 in [18]		3	6.4%	1.86 dB	101	0.84 λ_g × 0.41 λ_g
Partial H-plane SIW Filter in [24]		5	8%	1.98 dB	176	3.86 λ_g × 0.41 λ_g
FSIW filter in [29]		4	6%	2.62 dB	125	0.68 λ_g × 0.67 λ_g
Conventional Half-wavelength SIR filter in [30]		3	5.5%	2.14 dB	102	0.6 λ_g × 0.57 λ_g
This work	For bonding film with loss tangent of 0.02	4	6.2%	4.3 dB	73	0.68 λ_g × 0.21 λ_g
	For bonding film with loss tangent of 0.003	4	6.2%	1.8 dB	176	0.68 λ_g × 0.21 λ_g

Note: the Q_u is evaluated based on the filter insertion loss and bandwidth by using the experimental formula given in [27], and a Chebyshev lowpass prototype with a ripple level of 0.04 dB is assumed for all filters.

gives the comparison among the proposed work, the conventional partial H-plane SIW filters, the SIW-CRLH filters, the FSIW cavity filter, and the half-wavelength stepped-impedance-resonator (SIR) filter. From this table, it is clear that the proposed FSIW-CRLH partial H-plane filter has been size-reduced more than 80% as compared to the conventional partial H-plane SIW filters [24], and more than 59% as compared to the conventional SIW-CRLH filter [18], the FSIW cavity filter [29], and the half-wavelength SIR filter [30]. Moreover, even with a very lossy bonding film with the dielectric loss tangent of 0.02, the unloaded quality factor of the proposed resonator is comparable to those of the conventional SIW-CRLH filters. If the dielectric loss tangent of the bonding film decreases to 0.003, which is available in the industry, the unloaded quality factor of the proposed resonator will be much higher than the conventional SIW-CRLH resonators [18], the FSIW cavity resonator [29], and the half-wavelength SIR [30]. The high unloaded quality factor of the proposed resonator is benefited from the compact resonator size that introduces less dielectric and conductor losses. Meanwhile, the suppression of the fast-wave radiation loss contributes to a much higher unloaded quality factor as compared to the previous open SIW-CRLH resonators.

Due to the restriction of the fabrication technique, the manufacturing tolerances may influence the performance of the filter. To investigate the filter sensitivity to fabrication tolerances, the parameter studies were carried out in the EM simulator (Ansoft HFSS). The width (*wf*) of interdigital fingers, the slot size (*ws*) between the interdigital fingers and the thickness (t_1) of the bonding film are chosen as the variables and a 10% variation for each parameter was applied. Fig. 15 presents the simulated performance of the filter versus the variations of these physical dimensions. Only the simulated reflection coefficients $(|S_{11}|)$

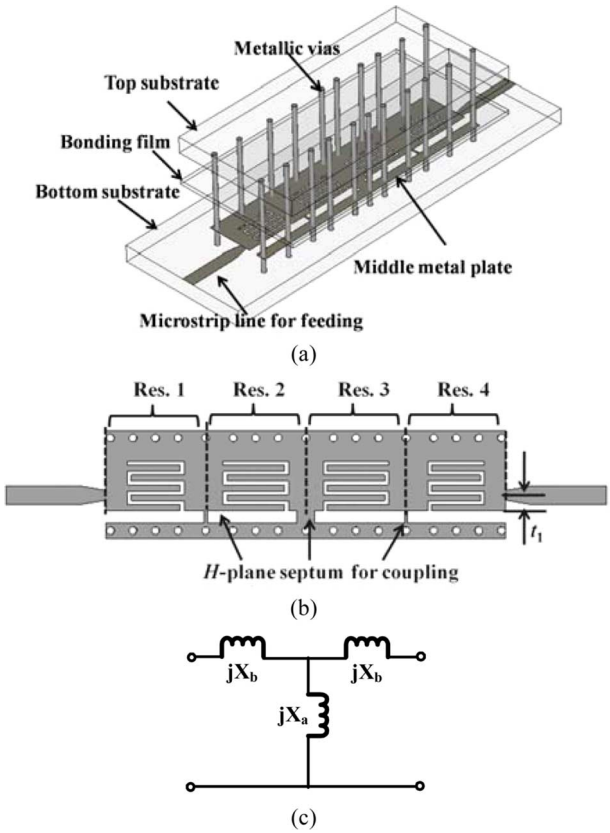

Fig. 16. Second type of the partial H-plane filters with the H-plane septa. (a) 3-D view. (b) Top view of the middle metal plate. (c) Equivalent circuit for the H-plane septa.

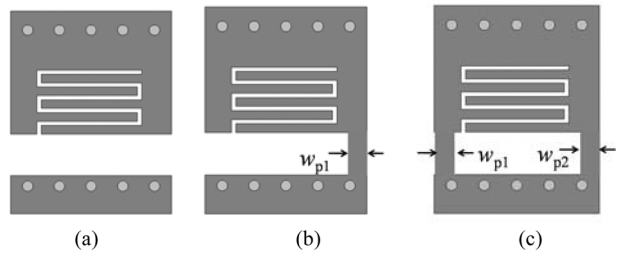

Fig. 17. (a) Resonator with two open ends. (b) Resonator with one H-plane septum and one open end. (c) Resonator with two H-plane septa.

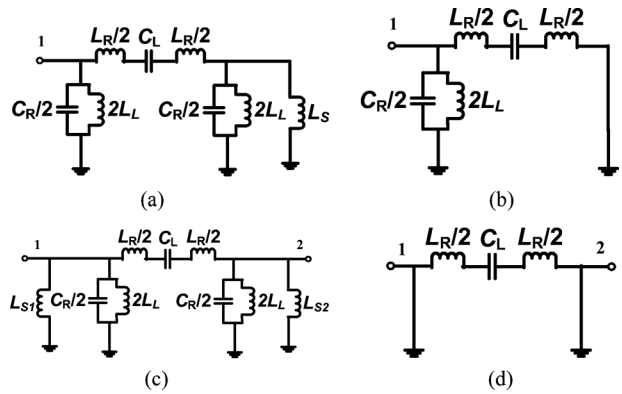

Fig. 18. (a) Equivalent circuit for the Res. 1 and Res. 4. (b) CRLH quarter-wave resonator. (c) Equivalent circuit for Res. 2 and Res. 3. (d) Zeroth order resonator.

of the filter are shown here for clarity. As can be observed, the $|S_{11}|$ in the passband is below -15 dB within the 10% variation for each parameter sweep. A frequency shift that is less than 1% of the center frequency is observed for the variation of *ws* and t_1 while a bandwidth reduction of less than 0.7% of the center frequency occurs versus the variation of *wf*. The filter performance shows well acceptable deterioration due to the parameter variations and is therefore concluded insusceptible to the fabrication tolerances.

B. Fourth-Order Bandpass Filter With H-Plane Septa

Fig. 16(a) gives the second type of the bandpass filter based on the proposed FSIW-CRLH structure. It also consists of four CRLH unit cells from Fig. 3 which are indicated as Res. 1, Res. 2, Res. 3, and Res. 4 in Fig. 16(b), respectively. Different from the filter in Fig. 9, an H-plane septum is introduced for interstage coupling between adjacent resonators. The H-plane septa can be modeled as a T-type network shown in Fig. 16(c) [26]. The values of the reactance in the equivalent circuit can be adjusted by varying the length of the septa, which is equal to the gap width (*wg*) of the FSIW in Fig. 3(b), and the width of septa. Two tapped microstrip lines are used as the input/output ports. The top substrate is made to be shorter than the bottom substrate for the access of the microstrip feeding lines.

Different from the resonators with the open-ended boundary condition in Fig. 9(b), the H-plane septum in Fig. 16(b) imposes a low-impedance boundary condition to the resonators at the place where it locates, and this is similar to the rectangular waveguide case in [21]. The imposed boundary condition will change the resonant frequencies of the original resonators. Considering only the direction of wave propagation in the filter, the Res. 1 and Res. 4 are open-ended at the sides where the input and output line are placed, and have a low-impedance end at the side where the H-plane septum is inserted, as shown in Fig. 17(b). Based on these boundary conditions, the equivalent circuit for these two resonators can be equivalent to the circuit shown in Fig. 18(a) where the equivalent inductance $L_{\rm s}$ represents the contribution from the H-plane septum. This inductance will make the first fundamental resonant frequency become higher than the frequency where $\beta d = -\pi$ in the previous dispersion diagram. In the extreme case, the equivalent circuit in Fig. 18(a) will become as the circuit in Fig. 18(b) when the inductance $L_{\rm s}$ is very small and can be neglected as a short circuit. In this case, the resulted resonator will become as the CRLH quarter-wave resonator with an electric length of $-\pi/2$ as elaborated in our previous studies [31] and [32]. Similarly, the Res. 2 and Res. 3 with two H-plane septa on either side as shown in Fig. 17(c) can be equivalent to the circuit shown in Fig. 18(c) with the side inductances $L_{\rm s1}$ and $L_{\rm s2}$. Therefore, the first fundamental resonant frequency of the Res. 2 and Res. 3 here will be much higher than the frequency where $\beta {\rm d} = -\pi$ in the dispersion diagram, and in the extreme case when the $L_{\rm s1}$ and $L_{\rm s2}$ are small enough, the equivalent circuit will become as the circuit in Fig. 18(d), which has a zeroth order resonance at the series resonant frequency of (2) [4].

To give a better understanding on the resonances of the proposed resonators, Table IV illustrates the first two fundamental resonant frequencies of the three different resonators shown in Fig. 17. All of the resonators have the same physical dimensions as given in Table II except the septa. The widths of

TABLE IV
FIRST TWO FUNDAMENTAL RESONANT FREQUENCIES OF THE RESONATORS IN FIG. 17

	First Resonance	*Second Resonance*
Resonator in Fig. 17 (a)	5.3 GHz	7.1 GHz
Resonator in Fig. 17 (b)	5.93 GHz	8.79 GHz
Resonator in Fig. 17 (c)	6.65 GHz	9.7 GHz

TABLE V
PHYSICAL DIMENSIONS OF RESONATORS IN THE SECOND TYPE OF THE PARTIAL H-PLANE FILTERS. UNIT: MIMMILETERS

	d	*lf*	*wc*	*wf*	*dv*	*wg*	*ws*	*wt*	w_{p1}	w_{p2}	*h*
Res. 1 and 4	7.2	3.8	5.7	0.5	0.8	0.7	0.2	1.2	0.105	N.A.	0.508
Res. 2 and 3	7.2	4.5	5.7	0.5	0.8	0.7	0.2	1.2	0.105	0.9	0.508

the septa in the resonators of Fig. 17(b) and (c) are chosen as $w_{\rm p1} = w_{\rm p2} = 0.12$ mm. From Table IV, it can be clearly observed that the resonant frequencies of the proposed resonator increases as the H-plane septa are added. Thus, the resonators in the filter of Fig. 16 need to be designed separately to resonate at the same frequency. This process can be done by adjusting the length of the interdigital fingers in the resonators.

The center frequency for the filter in Fig. 16 is also designed at 5.3 GHz. The physical dimensions of the resonators are shown in Table V. A Chebyshev low-pass prototype with a ripple level of 0.04 dB and a fractional bandwidth of 10% is used for this filter design, and the direct-coupling method in [27] is also applied for the design procedure. The filter schematic diagram can be also referred to Fig. 10(b). The interstage coupling can be adjusted by the width of the H-plane septa while the external quality factor can be tuned by changing the tapped position. The calculated interstage coupling matrix M and the external quality factor $Q_{\rm e}$ according to the low-pass prototype is given in (13)

$$M = \begin{bmatrix} 0 & 0.092 & 0 & 0 \\ 0.092 & 0 & 0.071 & 0 \\ 0 & 0.071 & 0 & 0.092 \\ 0 & 0 & 0.092 & 0 \end{bmatrix} \quad Q_e = 9.17. \quad (13)$$

Fig. 19 shows the extracted interstage coupling coefficients and the external quality factor with respect to the corresponding physical dimensions. As previously mentioned, the interstage coupling between resonators depends on the value of the reactance coming from the septa. When the widths (w_{p1} and w_{p2}) of the septa are small, the equivalent reactance of these septa is inductive and will decrease as their widths become larger. The resulted inductive coupling will be monotonically decreased as w_{p1} and w_{p2} become larger, given the length (*wg*) of the septa is fixed. However, when w_{p1} and w_{p2} increase to a certain value, the reactance will not be dominated again by the inductive effect of the septum due to the distribution effect and may become capacitive, and the resulted coupling may begin to increase due to the capacitive effect of the septa. Thus, a minimum coupling value between resonators 1 and 2 is observed at $wp_1 = 0.7$ mm in Fig. 19. This limited value of coupling could be decreased by decreasing the length (*wg*) of the septum. After the interstage coupling coefficients and the external quality factor being extracted, the physical dimension for the required coupling coefficients and $Q_{\rm e}$ in (13) can be directly read from Fig. 19.

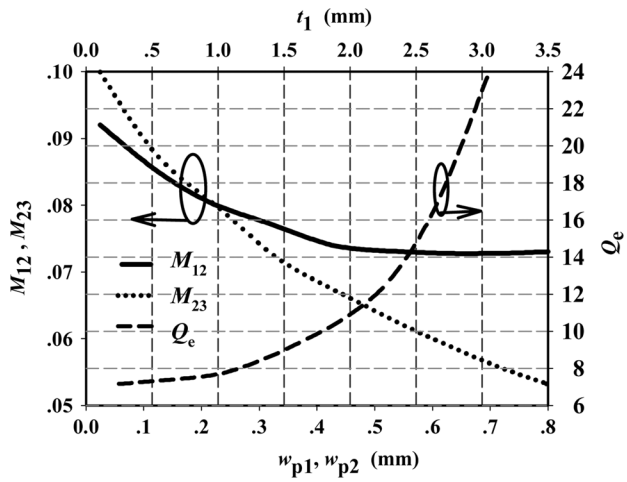

Fig. 19. Extracted interstage coupling coefficients and external quality factor for input/output coupling. Here, M_{12} is the coupling between Res. 1 and Res. 2, M_{23} is the coupling between Res. 2 and Res. 3, and the length (*wg*) of the septum is fixed to be 1 mm for calculation.

The filter was fabricated using the same substrate and the same bonding film as in the previous case of the filter with the H-plane slots. Fig. 20 shows the simulated and measured filter performances. As observed, good agreement between the simulation and measurement is observed. The center frequency is at 5.3 GHz and the 3 dB fractional bandwidth is about 10%. The reflection coefficients are less than -15 dB in the passband for both the simulation and measurement. The minimum insertion loss for simulation is about 2.2 dB while it is about 2.7 dB in the measurement. The discrepancy between the simulation and measurement is due to the deviations of the dielectric loss tangents of the substrate and the bonding film, and the connector loss that is not included in the simulation. Again, the high insertion losses obtained in both the simulation and measurement are due to the high loss factor of the bonding film between the top and bottom substrates. It is found that the insertion loss will be improved by nearly 1.2 dB if the bonding film with a dielectric loss tangent of 0.003 is used. Fig. 21 gives the wide-band response of the measured $|S_{21}|$. The first two spurious passbands are observed at around 7 and 8 GHz. These two spurious passbands correspond to the second resonant frequencies of the Res. 1 (or Res. 4) and Res. 2 (or Res. 3), respectively. Another two higher spurious passbands are observed around 9 and 10 GHz,

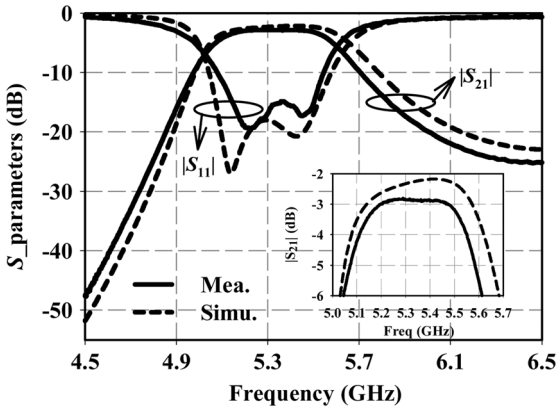

Fig. 20. Simulated and measured results of the second type of the partial H-plane filters with H-plane septa.

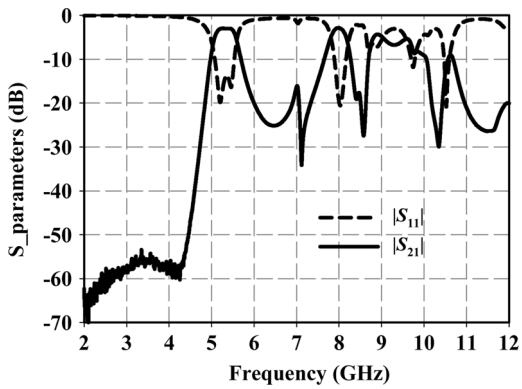

Fig. 21. Measured wide-band responses of the second type of the partial H-plane filters.

respectively. These two passbands may result from the third fundamental resonances of the two types of resonators in the filter.

The size of this filter is about 28.8 $\times$7.6 mm $(0.75\lambda_g \times 0.20\lambda_g)$, which is slightly longer than the first type of the partial H-plane filter due to the size increase of the resonators with the H-plane septa. However, the overall footprint size of the second type of the partial H-plane filters is still much smaller than the conventional FSIW partial H-plane filters in [23] and [24] and conventional SIW-CRLH filters in [18].

V. Conclusion

In this paper, a CRLH transmission structure based on the FSIW is presented and discussed. The proposed FSIW-CRLH structure exhibits much lower cut-off frequency as compared to the conventional FSIW structures, offering the advantage of miniaturization. Furthermore, benefited from its closed structural feature, the proposed FSIW-based CRLH transmission structure is able to suppress the fast-wave radiation that exists in the previously open CRLH transmission lines, resulting in the proposed structure with a higher quality factor and better electromagnetic compatibility from the system design point of view. Two types of the partial H-plane filters based on the proposed FSIW-CRLH resonators were realized to support our idea. Both the theoretic and experimental results are given, and agree well with each other. The resultant filters have demonstrated more than 80% size reduction as compared to the conventional FSIW partial H-plane filters, and more than one-half size reduction to the conventional SIW-CRLH filters. The proposed resonators are expected to have much higher unloaded quality factor than both the conventional FSIW resonators and SIW-CRLH resonators when less lossy bonding films are used.

References

[1] V. G. Veselago, "The electrodynamics of substances with simultaneously negative values of "ε and μ.," *Sov. Phys.—Usp.*, vol. 10, no. 4, pp. 509–514, Jan.–Feb. 1968.

[2] J. B. Pendry, A. J. Holden, D. J. Robbins, and W. J. Stewart, "Low frequency plasmons in thin-wire structures," *J. Phys., Condens. Matter*, vol. 10, pp. 4785–4809, Mar. 1998.

[3] G. V. Eleftheriades and K. G. Balmain, *Negative Refraction Metamaterials: Fundamental Properties and Applications*. Hoboken, NJ: Wiley, 2005.

[4] C. Caloz and T. Itoh, *Electromagnetic Metamaterials*. New York: Wiley, 2005.

[5] C. Caloz and T. Itoh, "Transmission line approach of left-handed (LH) materials and microstrip implementation of an artificial LH transmission line," *IEEE Trans. Antennas Propag.*, vol. 52, no. 5, pp. 1159–1166, May 2004.

[6] G. V. Eleftheriades, A. K. Iyer, and P. C. Kremer, "Planar negative refractive index media using periodically L-C loaded transmission lines," *IEEE Trans. Microw. Theory Tech.*, vol. 50, no. 12, pp. 2702–2712, Dec. 2002.

[7] T. Decoopman, A. Marteau, E. Lheurette, O. Vanbesien, and D. Lippens, "Left-handed electromagnetic properties of split-ring resonator and wire loaded transmission line in a fin-line technology," *IEEE Trans. Microw. Theory Tech.*, vol. 54, no. 4, pp. 1451–1457, Apr. 2006.

[8] S. Hrabar, J. Bartolic, and Z. Sipus, "Waveguide miniaturization using uniaxial negative permeability metamaterial," *IEEE Trans. Antennas Propag.*, vol. 53, no. 1, pp. 110–119, Jan. 2005.

[9] Y. Dong and T. Itoh, "Composite right/left-handed substrate integrated waveguide leaky-wave antennas," in *Proc. 39th Eur. Microw. Conf.*, 2009, pp. 276–279.

[10] Y. Dong, T. Yang, and T. Itoh, "Substrate integrated waveguide loaded by complementary split-ring resonators and its applications to miniaturized waveguide filters," *IEEE Trans. Microw. Theory Tech.*, vol. 57, no. 9, pp. 2211–2223, Sep. 2009.

[11] Y. Dong and T. Itoh, "Composite right/left-handed substrate integrated waveguide and half mode substrate integrated waveguide leaky-wave structures," *IEEE Trans. Antennas Propag.*, vol. 59, no. 3, pp. 767–775, Mar. 2011.

[12] Y. Dong and T. Itoh, "Substrate integrated composite right/left-handed leaky-wave structure for polarization-flexible antenna application," *IEEE Trans. Antennas Propag.*, vol. 60, no. 2, pp. 760–771, Feb. 2012.

[13] T. Yang, P.-L. Chi, and R. Xu, "Novel composite right/left-handed leaky-wave antennas based on the folded substrate-integrated-waveguide structures," *Progr. Electromagn. Res. C*, vol. 29, pp. 235–248, 2012.

[14] T. Kodera and C. Caloz, "Uniform ferrite-loaded open waveguide structure with CRLH response and its application to a novel backfire-to-endfire leaky-wave antenna," *IEEE Trans. Microw. Theory Tech.*, vol. 57, no. 4, pp. 784–795, Apr. 2009.

[15] C. Caloz, A. Sanada, and T. Itoh, "A novel composite right-/left-handed coupled-line directional coupler with arbitrary coupling level and broad bandwidth," *IEEE Trans. Microw. Theory Tech.*, vol. 52, no. 3, pp. 980–992, Mar. 2004.

[16] A. Hirota, Y. Tahara, and N. Yoneda, "A compact forward coupler using coupled composite right-/left-handed lines," *IEEE Trans. Microw. Theory Tech.*, vol. 57, no. 12, pp. 3127–3133, Dec. 2009.

[17] C. Liu and W. Menzel, "Broadband via-free microstrip balun using metamaterial transmission lines," *IEEE Microw. Wireless Compon. Lett.*, vol. 18, no. 7, pp. 437–439, Jul. 2008.

[18] Y. Dong and T. Itoh, "Substrate integrated waveguide negative-order resonances and their applications," *IET Microw. Antennas Propag.*, vol. 4, no. 8, pp. 1081–1091, Aug. 2010.

[19] G. H. Zhai, W. Hong, K. Wu, J. X. Chen, P. Chen, J. Wei, and H. J. Tang, "Folded half mode substrate integrated waveguide 3 dB coupler," *IEEE Microw. Wireless Compon. Lett.*, vol. 18, no. 8, pp. 101–103, Feb. 2008.

[20] W. Che, L. Geng, K. Deng, and Y.-L. Chow, "Analysis and experiments of compact folded substrate-integrated waveguide," *IEEE Trans. Microw. Theory Tech.*, vol. 56, no. 1, pp. 88–93, Jan. 2008.

[21] D.-W. Kim, D.-J. Kim, and J.-H. Lee, "Compact partial H-plane filters," *IEEE Trans. Microw. Theory Tech.*, vol. 54, no. 11, pp. 3923–3930, Nov. 2006.
[22] D.-J. Kim and J.-H. Lee, "Partial H-planer filters with multiple transmission zeros," *IEEE Trans. Microw. Theory Tech.*, vol. 56, no. 7, pp. 1693–1698, Jul. 2008.
[23] Z. Wang, D. Shen, R. Xu, W. Lin, Y. Guo, and X. Xie, "Partial H-Plane bandpass filters based on substrate integrated folded waveguide (SIFW)," in *Proc. Asia-Pac. Microw. Conf.*, 2009, pp. 2545–2548.
[24] H. Aghayari and N. Komjani, "Substrate integrated waveguide *H*-plane filter," in *Proc. 39th Eur. Microw. Conf.*, 2009, pp. 460–463.
[25] D. M. Pozar, *Mirowave Engineering*, 3rd ed. Hoboken, NJ: Wiley, 2005, pp. 372–374.
[26] G. Matthaei, E. Jones, and L. Young, *Microwave Filters, Impedance Matching Networks, and Coupling Structures*. Norwood, MA: Artech House, 1980, pp. 421–487.
[27] J. S. Hong and M. J. Lancaster, *Microstrip Filter For RF/Microwave Applications*. Hoboken, NJ: Wiley, 2001.
[28] Rogers Corporation [Online]. Available: http://www. rogerscorp.com/acm/products/13/3001-Bonding-Film-Thermoplastic-Chloro-fluorocopolymer.aspx
[29] R. Wang, L.-S. Wu, and X.-L. Zhou, "Comapct folded substrate integrated waveguide cavity and bandpass filter," *Progr. Electromagn. Res.*, vol. 84, pp. 135–147, 2008.
[30] R.-J. Mao, X.-H. Tang, L. Wang, and G.-H. Du, "Miniaturized hexagonal stepped-impedance resonators and their applications to filters," *IEEE Trans. Microw. Theory Tech.*, vol. 56, no. 2, pp. 440–448, Feb. 2008.
[31] T. Yang, P.-L. Chi, and T. Itoh, "Compact quarter-wave resonator and its applications to miniaturized diplexer and triplexer," *IEEE Trans. Microw. Theory Tech.*, vol. 59, no. 2, pp. 260–269, Feb. 2011.
[32] T. Yang, M. Tamura, and T. Itoh, "Compact hybrid resonator with series and shunt resonances used in miniaturized filters and balun filters," *IEEE Trans. Microw. Theory Tech.*, vol. 58, no. 2, pp. 390–402, Feb. 2010.

Tao Yang (S'09–M'11) received the B.Eng. and Ph.D. degrees from the University of Electronic Science and Technology of China, Chengdu, China, in 2005 and 2011, respectively.

Since July 2011, he has been a Lecturer with University of Electronic Science and Technology of China. From September 2008 to September 2010, he was a visiting Scholar with the Electrical Engineering Department, University of California at Los Angeles (UCLA). From August 2011 to September 2012, he was a Postdoctoral Researcher with the Institut d'Electronique et de Telecommunications de Rennes (IETR) and Université de Rennes 1, Rennes, France. Currently, he is a Postdoctoral Researcher in Department of Electrical and Computer Engineering, University of California, San Diego (UCSD). His research includes the Ka-band circuit designs such as Ka-band frequency synthesizer and transceiver; miniaturized passive microwave and millimeter wave components such as filter, diplexer, triplexer, and baluns; broadband microstrip antennas and leaky-wave antennas; metamaterial-based microwave circuits; and low temperature cofired ceramic (LTCC) technology.

Pei-Ling Chi (S'08–M'11) received the B.S. and M.S. degrees in communication engineering from the National Chiao Tung University, Hsinchu, Taiwan, in 2004 and 2006, respectively, and the Ph.D. degree in electrical engineering from the University of California at Los Angeles, in 2011.

Since 2011, she has been with the National Chiao Tung University as Assistant Professor of Electrical and Computer Engineering. She holds several U.S. and international patents in the area of the left-handed metamaterials. Her research interests include the analysis and design of the left-handed metamaterial circuits, the phased-array transceiver development, and implementation of RF/microwave components and integrated systems.

Dr. Chi was the recipient of the Research Creativity Award from National Science Council, Taiwan, in 2004.

Ruimin Xu received the B.S., M.S., and Ph.D. degrees from the University of Electronic Science and Technology of China (UESTC), Chengdu, China, in 1982, 1987, and 2008, respectively.

From November 1993 to May 1996, he was appointed to attend advanced study and work with the Agilis Communication Corporation of the Singapore Science and Technology Group by UESTC, during which time he mainly took charge of research in high frequency front-ends of the satellite ground VSAT system. In May 1996, he returned to UESTC. In 2000, he became a Full Professor with the School of Electrical Engineering, UESTC, and became the Director of the Microwave Engineering Department. His current research interests include microwave and millimeter-wave circuits and systems.

Weigan Lin (M'86–SM'91) received the M.S. and Ph.D. degrees from the University of California at Berkeley in 1947 and 1950, respectively.

He has been a Visiting Professor with the University of California at Berkeley; the University of Kyushu, Kyushu, Japan; Mantoba University, Winnipeg, MB, Canada; and the City University of Hong Kong. As lead author, he has authored many scientific and technical books, including *Microwave Network* (National Defense Industry Press, 1978), *Microwaves Theory and Technology* (Science Press, 1979), *Electromagnetic Field Theory* (National Defense Industry Press, 1984). He also also authored or coauthored over 200 papers in journals and conferences. His research field includes electromagnetic theory and application.

Prof. Lin is a Fellow of the Chinese Institute of Electronics (CIE). He is chief of the IEEE Microwave Theory and Techniques Society (IEEE MTT-S) Beijing Branch. In 1980, he was elected as a member of the Academy of Science of China. He has been honored as the "Father of Microwave in China" due to his scientific contributions. He has also been the recipient of many awards, including the National Natural Science Progress Prize, over 10 prizes awarded by the Ministries of China, and the HeliangHeli Foundation Award for Science and Technology (1999).